Towards a quantum Monte Carlo for lattice systems

S. Figueroa-Manrique, and K. Rodríguez-Ramírez
Departamento de Física, Universidad del Valle, A.A. 25360, Cali, Colombia.
e-mail: santiago.figueroa@correounivalle.edu.co

K. Rodríguez-Ramírez
Departamento de Física, Universidad del Valle, A.A. 25360, Cali, Colombia.
Centre for Bioinformatics and Photonics-CiBioFi, Calle 13 No. 100-00, Edificio 320 No. 1069, Cali, Colombia

In this work we build the foundations of a quantum Monte Carlo as a stochastic numerical method to solve lattice many-body quantum systems with nearest-neighbor interactions at most. As motivation, we briefly describe the bilinear-biquadratic Heisenberg model with an external field, for spin-1 particles, as an effective Hamiltonian of the Bose-Hubbard model with an external quadratic Zeeman field in the Mott insulator phase at unit filling. Then, we discuss how to implement the world line Monte Carlo with local updates to circumvent the difficulties that arise on these type of systems by mapping the quantum partition function into the one of an effective classical model, in one additional dimension, given by the imaginary time evolution of the system. Such a mapping is performed by means of the Suzuki-Trotter decomposition, which transforms the original partition function into a summation of weights given by the classical configurations. Later, we present a set of observables that can be measured through this method and show how to use a Metropolis update scheme to accomplish the measurements. At last, we present the maximization of the configuration weights for three parameter sets as the first and relevant step to perform future measurements.

Keywords: Quantum Monte Carlo; spin-1 system; Heisenberg model; optical lattices.

En este trabajo se contruyen los fundamentos de un Monte Carlo cuántico como método numérico estocástico para resolver sistemas cuánticos reticulares de muchos cuerpos con interacción a primeros vecinos a lo sumo. Como motivación, describimos brevemente el modelo de Heisenberg bilineal-bicuadrático con un campo externo, para partículas de espín 1, como el hamiltoniano efectivo del modelo de Bose-Hubbard con un campo de Zeeman cuadrático externo en la fase de aislante de Mott con una partícula por sitio de red. Posteriormente, discutimos como implementar el *world line* Monte Carlo con actualizaciones locales para evitar las dificultades que surgen en este tipo de sistemas al mapear la función de partición cuántica en la de un modelo clásico efectivo en una dimensión adicional dada por la evolución imaginaria del sistema. Dicho mapeo es realizado a través de la descomposición de Suzuki-Trotter, la cual transforma la función de partición original en la suma de pesos dados por las configuraciones clásicas. A continuación, presentamos un conjunto de observables que pueden ser medidas utilizando este método y mostramos como usar el esquema de actualizaciones locales del algorítmo de Metrópolis para obterner las medidas. Finalmente, mostramos la maximización de los pesos de las configuraciones clásicas para tres conjuntos de parámetros como primer y relevante paso para desarrollar futuras mediciones.

Descriptores: Monte Carlo cuántico; sistemas de espín 1; modelo de Heisenberg; redes ópticas.

PACS: 02.70.Ss; 05.30.Jp; 03.75.Mn; 67.85-d

1. Introduction

Ultracold gases in optical lattices are an important tool to study strongly correlated systems under very controlled conditions [1, 2], as it was highlighted in the theoretical prediction [3] and later in the experimental realization of the phase transition from superfluid to Mott insulator in bosonic systems at ultralow temperatures [4]. The achievement of such low temperatures is very remarkable, as it has boosted different experimental, theoretical and numerical progress, such that multiple Nobel prizes have been awarded in the last two decades [5–11].

Due to the experimental progress, today it is possible to build a perfect periodic potential using counter-propagating lasers [1, 2]. These light potentials constitute the optical lattices, which take the role of a perfect crystal lattice and thus can be loaded with different types of particles such as ultracold bosons. As a result, optical lattices with ultracold par-

ticles present a very high degree of control in the set of parameters and constitute extraordinary tools as quantum simulators [1, 12, 13].

On the other hand, adding spin to the particles is of great interest, because the inclusion of internal degrees of freedom leads to very rich ground-state physics, such as new quantum phases [14–17, 26] and quantum magnetism [19, 20]. Spin-1 bosons in optical lattices are particularly fascinating, because they are the simplest spinor system beyond the usual spin-1/2 to exhibit spin changing collisions, hence they are ideal to study quantum magnetism [19, 20] and multiple novel quantum phase transitions [21–24]. Likewise, the quadratic Zeeman effect (QZE) plays a significant role in reticular spinor systems [25–27], but its role in the phases of such systems with spin-1 remains largely unexplored.

The study of many-body quantum phenomena becomes non-trivial and the number of problems with an exact solution is very limited; particularly, reticular bosonic sys-

tems only have exact analytical solution at certain specific points where high symmetry is exhibited [28]. Also, due to the exponential growth of the Hilbert space with respect to the number of particles, the internal degrees of freedom and the lattice sites, the use of special numerical methods is mandatory. Some of the most commonly used are Quantum Monte Carlo (QMC) [29–31], Density Matrix Renormalization Group (DMRG) [32, 33], Bethe *ansatz* [34], Gutzwiller *ansatz* [35], among others.

The paper is organized in the following way: In Sec. 2, we present a brief review of the physical system under consideration, which is the spin-1 bilinear-biquadratic Heisenberg model with an external quadratic Zeeman field. In Sec. 3, a description of the world line Monte Carlo with local updates for one-dimensional lattice systems is made. In Sec. 4, the measurement of observables and the local update scheme based on the Metropolis algorithm are explained. In Sec. 5, we present the maximization of the configurations weights as a relevant and primary accomplishment towards the Monte Carlo measurement of allowed physical observables. Finally, the conclusions of this work are presented in Sec. 6.

2. Heisenberg model

The Bose-Hubbard model is the simplest non-trivial model that describes strongly correlated spin-1 bosons in a periodic potential, which here is taken as an optical lattice [1, 2]. This model presents two quantum phases, the Mott insulator and the superfluid phases [1, 2]. We consider repulsively interacting ultracold spin-1 bosons in a d-dimensional hypercubic lattice prepared in a balanced mixture, *i.e.* keeping the magnetization to zero. At unit filling, the system is in the Mott insulator regime when the on-site interactions dominate (U_0, U_2) over the hopping amplitude (t) between nearest-neighboring sites. In second-order perturbation theory in the hopping, the low-energy physics is given by superexchange processes, being described by an effective spin Hamiltonian [25], which in the presence of an external quadratic Zeeman field is the bilinear-biquadratic Heisenberg model given by

$$\hat{H} = \sum_{\langle i,j \rangle} \left[\cos\theta \left(\hat{\vec{S}}_i \cdot \hat{\vec{S}}_j \right) + \sin\theta \left(\hat{\vec{S}}_i \cdot \hat{\vec{S}}_j \right)^2 \right]$$
$$- D \sum_i \left(\hat{S}_i^z \right)^2, \tag{1}$$

where the $\langle i,j \rangle$ notation refers to the summation over nearest neighbors only; $\hat{\vec{S}}_i$ are the single-particle spin-1 vector operators of the *i-th* lattice site $\hat{\vec{S}}_i =: (\hat{S}_i^x, \hat{S}_i^y, \hat{S}_i^z)$, with $\hbar = 1$; θ is a parameter that in our considerations comes from the Bose-Hubbard on-site interactions and determines the spin-spin strengths:

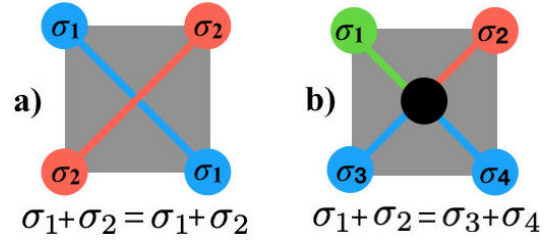$$\tan\theta = \frac{U_0 + 2U_2}{3U_0}, \tag{2}$$

FIGURE 1. a) Spin preserving collisions. b) Spin changing collisions.

with $U_0 = (4\pi\hbar^2 a_0/m)$ and $U_2 = 4\pi\hbar^2 a_2/m$ the interaction strengths of the two possible completely symmetric allowed collision channels with total spin $F = \{0, 2\}$, where a_F are the s-wave scattering lengths of each channel and m the mass of the particles. The last term of D, is the parametrized quadratic Zeeman field.

The Heisenberg model in Eq. (1) presents rich ground-state physics and quantum magnetism [25]. This model exhibits two different types of collisions, one that preserves the spin projection and one that does not. Fig. 1 shows a scheme of these processes: a) the two incoming particles (top) interact (lines crossing), resulting on two final particles (bottom) with the same spin projections σ; b) in the second case, the black dot represents a spin changing collision: the interaction between the initial particles yields two particles that have changed spin projections. Albeit, the total spin projection before and after the interaction must be conserved $\sigma_1 + \sigma_2 = \sigma_3 + \sigma_4$.

On the other hand, the external quadratic field favors the energy minimization for different states, depending on its sign and strength. For $D = 0$, states with projection -1, 0, and 1 minimize the energy equally; on the contrary, projections -1 and 1 are favored when $D > 0$, and projection 0 is favored when $D < 0$.

Finally, to study this Heisenberg model, we use the basis of the local spin magnetic projection operators $\hat{S}_i^z$ (with z the quantization axis) for spin-1 bosons:

$$\{|S_i^z \equiv \sigma_i\rangle\} = \{|-1\rangle, |0\rangle, |1\rangle\}. \tag{3}$$

A more extensive review of the Heisenberg model is found in [1, 36].

3. World line Monte Carlo

The study of interacting many-body quantum problems is a challenging task, principally due to the exponential growth of their basis with respect to the number of particles and degrees of freedom. For example, since the basis of the spin-1 model grows as 3^N, the size grows up to $\approx 10^{80}$ for only 168 particles, which is approximately the number of atoms in the visible universe.

However, there are different methods to study this type of systems. In particular, the world line Monte Carlo [17,26,27] is a stochastic numerical method (of the quantum Monte

Carlo type) that circumvents the difficulties that arise by first, mapping the quantum partition function of the original d-dimensional system into the one of an effective d+1 classical model and then, implementing a statistical sampling on the new partition function.

Let us start with the mapping of the partition function. For this purpose, we perform the Suzuki-Trotter decomposition [37], by first introducing the Trotter approximation [38]. Let $\hat{A}$ and $\hat{B}$ be two bounded operators such that $[\hat{A}, \hat{B}] \neq 0$ and let x be an arbitrary parameter. The Trotter approximation is then given by

$$e^{x\hat{A}}e^{x\hat{B}} = e^{x(\hat{A}+\hat{B})+\mathcal{O}(x^2)}, \tag{4}$$

with $\mathcal{O}(x^2)$ an error of second order.

Now, we recall the bilinear-biquadratic Heisenberg Hamiltonian for spin-1 particles in Eq. (1). Since we only consider nearest neighbor interactions, the Hamiltonian can be separated as follows

$$\hat{H} = \sum_i \hat{H}_{i,i+1}, \tag{5}$$

with $\hat{H}_{i,i+1}$ the bond Hamiltonians between sites i and $i + 1$. Due to the short range interactions, we distinguish two classes of bonds Hamiltonians, even and odd, such that

$$\hat{H} = \sum_{i\ even} \hat{H}_{i,i+1} + \sum_{i\ odd} \hat{H}_{i,i+1} = \hat{H}_A + \hat{H}_B. \tag{6}$$

This leads to two useful properties: The first is that $[\hat{H}_A\hat{H}_B] \neq 0$ as a result of the nearest neighbor interactions; the second, is that the bond Hamiltonians commute with each other $[\hat{H}_{i,i+1}^{A(B)}\hat{H}_{j,j+1}^{A(B)}] = 0$ for i and j both even (or odd), because the two Hamiltonians act on different Hilbert spaces. As a result, we separate the Hamiltonian into two non-commuting parts, each of them made of a summation of commuting terms (which can be done to any Hamiltonian with nearest neighbor interactions at most).

Straightaway, we use the Trotter approximation to transform the partition function, such that $\hat{H}_A$ and $\hat{H}_B$ take the place of the non commuting unbounded operators:

$$Z = \mathrm{Tr}\, e^{-\beta\hat{H}} = \mathrm{Tr}\, e^{-\beta(\hat{H}_A+\hat{H}_B)} \approx \mathrm{Tr}\, e^{-\beta\hat{H}_A}e^{-\beta\hat{H}_B}, \tag{7}$$

where Tr is the trace operator, $\beta = (1/k_BT)$, k_B the Boltzmann constant and T the temperature of the system. Eq. (7) is known as the Suzuki-Trotter decomposition.

To get rid of the second order error given by the Trotter approximation, we introduce an integer M (the Trotter number) in the above expression and take the limit when M goes to infinity, thus the partition function becomes

$$Z = \lim_{M\to\infty} \mathrm{tr}\left(e^{-\Delta\tau\hat{H}_A}e^{-\Delta\tau\hat{H}_B}\right)^M, \tag{8}$$

where $\Delta\tau = \beta/M$ and $e^{-\Delta\tau\hat{H}_A}$ ($e^{-\Delta\tau\hat{H}_B}$) can be seen as imaginary time evolution operators through a Wick transformation [39]. The effect of these operators are discussed more

extensively later in the paper. On the other hand, it is clear that one can not numerically take the Trotter number to infinity, but what can be done is to run simulations with increasing Trotter numbers and perform a finite-size scaling.

To see the effect of the decomposition to the partition function, we express Eq. (8) as a product of $2M$ exponentials:

$$Z = \lim_{M\to\infty} \sum_{\sigma^0} \langle\sigma^0|\underbrace{e^{-\Delta\tau\hat{H}_A}}_{1}\underbrace{e^{-\Delta\tau\hat{H}_B}}_{2}\cdots$$
$$\times \underbrace{e^{-\Delta\tau\hat{H}_A}}_{2M-1}\underbrace{e^{-\Delta\tau\hat{H}_B}}_{2M}|\sigma^0\rangle. \tag{9}$$

The super-index in σ is annexed as a label, because several completeness relations must be added; in this way, the trace is always going to be identified by the 0-th super-index. Then, we add $2M - 1$ completeness relations $\sum_{\sigma^\alpha}|\sigma^\alpha\rangle\langle\sigma^\alpha|$, locating them between the product of exponentials and each one labeled accordingly. In addition, a short notation for the multiple summations is used. Then, the partition function becomes

$$Z = \lim_{M\to\infty} \sum_{\{\sigma\}} \underbrace{\langle\sigma^0|e^{-\Delta\tau\hat{H}_A}|\sigma^1\rangle}_{1}\underbrace{\langle\sigma^1|e^{-\Delta\tau\hat{H}_B}|\sigma^2\rangle}_{2}\cdots$$
$$\times \underbrace{\langle\sigma^{2M-2}|e^{-\Delta\tau\hat{H}_A}|\sigma^{2M-1}\rangle}_{2M-1}\underbrace{\langle\sigma^{2M-1}|e^{-\Delta\tau\hat{H}_B}|\sigma^0\rangle}_{2M}. \tag{10}$$

Because the Hamiltonians defining the exponentials of each matrix element in Eq. (10) are a summation of commuting bonds of two sites, these elements are separated in simple products regarding only exponentials of two sites Hamiltonians:

$$\langle\sigma^\alpha|e^{-\Delta\tau\hat{H}_{A(B)}}|\sigma^{\alpha+1}\rangle = \langle\sigma^\alpha|\prod_{i(j)}e^{-\Delta\tau\hat{H}_{i,i+1(j,j+1)}}|\sigma^{\alpha+1}\rangle$$
$$= \prod_{i(j)}\langle\sigma^\alpha_{i,i+1(j,j+1)}|e^{-\Delta\tau\hat{H}_{i,i+1(j,j+1)}}|\sigma^{\alpha+1}_{i,i+1(j,j+1)}\rangle, \tag{11}$$

with i (j) the even (odd) sites wherein the matrix elements are defined. From this point on, we refer to the two sites matrix elements defined in Eq. (11) as plaquettes, which are depicted in Fig. 1 by the shaded squares. Finally, the partition function is explicitly transformed into

$$Z = \lim_{M\to\infty} \sum_{\{\sigma\}}$$
$$\times \underbrace{\langle\sigma^0_{1,2}|e^{-\Delta\tau\hat{H}_{1,2}}|\sigma^1_{1,2}\rangle\cdots\langle\sigma^0_{N-1,N}|e^{-\Delta\tau\hat{H}_{N-1,N}}|\sigma^1_{N-1,N}\rangle}_{1}\cdots$$
$$\times \underbrace{\langle\sigma^{2M-1}_{2,3}|e^{-\Delta\tau\hat{H}_{2,3}}|\sigma^0_{2,3}\rangle\cdots\langle\sigma^{2M-1}_{N,1}|e^{-\Delta\tau\hat{H}_{N,1}}|\sigma^0_{N,1}\rangle}_{2M}, \tag{12}$$

or in a simplified form:

$$Z = \lim_{M \to \infty} \sum_{\{\sigma\}} \prod_{\alpha=0}^{2M-1} \prod_{i=1}^{N} \langle \sigma_{i,i+1}^{\alpha} | e^{-\Delta\tau \hat{H}_{i,i+1}} | \sigma_{i,i+1}^{\alpha+1} \rangle. \quad (13)$$

In both Eq. (12) and Eq. (13), periodic boundary conditions in the super-indexes and the sub-indexes are imposed by the trace and the choice of spatial periodic boundary conditions, respectively. From these expressions, it is clear that Z becomes a summation of real numbers given by the product of the plaquettes, rather than a summation of operators. Hence, the partition function of the original quantum system has been mapped into one of an effective classical model. Additionally, every adding in Z is an statistical weight given by one configuration of the effective model, which is determined by the product of plaquettes. Thereby, the partition function is determined as the summation of the weights defined by all the effective classical configurations:

$$Z = \sum_{C} \prod_{P} \Omega(C|P) = \sum_{C} \Omega(C), \quad (14)$$

where $\Omega(C|P)$ is the weight of a single plaquette (P) from a given classical configuration (C) with $\Omega(C)$ its total weight. However, evaluating directly this partition function is still impossible, because the number of possible classical configurations is even bigger than the original Hilbert space. Nonetheless, one can think of using importance sampling to obtain a good enough approximation in order to be able to measure estimators. This is discussed with more detail in Sec. 4..

We now focus on the classical mapping. Let us go back to the plaquette defined by Eq. (11) and recall that the exponential operator works as an imaginary-time evolution operator that propagates the two bonded particles in sites i (j) and $i + 1$ ($j + 1$) from configuration σ^{α} to configuration $\sigma^{\alpha+1}$. A classical configuration is determined by the imaginary-time evolution of all the particles, in $2M$ time steps, starting from an initial configuration σ^0, throughout multiple ones $\sigma^1 - \sigma^{2M-1}$ and back to the initial one σ^0, which means that the original d-dimensional quantum problem is mapped into d+1-dimensional classical one, with the imaginary time as the additional dimension settled by the Trotter number. The configurations are defined by the magnetic spin projections of the particles and the evolution is done alternating odd and even sites. However, not all possible configurations are allowed. On the one hand, for a finite size classical configuration (finite M), the boundary conditions imposed by the trace forbid certain configurations; on the other hand, only plaquettes given by the 19 non-zero matrix elements of the two-sites Hamiltonian are permitted, because the other ones would not give any statistical weight.

Keeping in mind the previous considerations, we draw, as an example, one classical configuration in Fig. 2 for the spin-1 bilinear-biquadratic Heisenberg chain with 6 lattice sites and $M = 3$. Blue, red and green dots represent particles with 0, 1 and -1 spin magnetic projection, respectively, that evolve in the vertical direction, from top to bottom in imaginary time. The continues lines represent the evolution of each
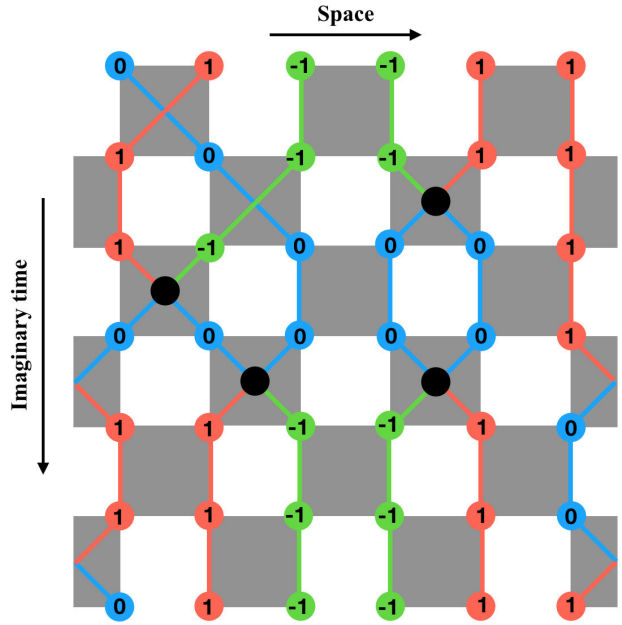

FIGURE 2. Classical configuration of the spin-1 bilinear-biquadratic Heisenberg chain with 6 lattice sites and $M = 3$. Blue, red and green dots represent particles with 0, 1 and -1 spin magnetic projection, respectively. The continues lines represent the world lines of each projection, and the shaded squares represent the plaquettes. The vertical axis is the imaginary time, and the horizontal is the spatial axis.

particle, these are the so-called world lines. The half-shaded squares at the edges account for the spatial boundary conditions in the horizontal axis. The Trotter number defines $2M$ imaginary time slices, half for the plaquettes of odd bonds and the other half for the plaquettes of even bonds.

By means of this graphic representation, the effect of the Suzuki-Trotter decomposition on the partition function is illustrated.

4. Observables

In this section, we describe the set of observables that we can measure through the new representation of the partition function defined by Eq. (14). First, since we use a statistical approach, we can only measure expected values of quasi-local observables and we can not calculate their individual eigenvalues, ruling out observables such as the von Newmann entropy with this approach. By construction, the observables need to be separable in the same sense as the Hamiltonian in Eq. (6), meaning that

$$\hat{O} = \sum_{i\ even} \hat{O}_{i,i+1} + \sum_{i\ odd} \hat{O}_{i,i+1} = \hat{O}_A + \hat{O}_B, \quad (15)$$

hence the accessible observables are those that can be written as sums of operators acting on two nearest neighbors at most. Additionally, the observables must locally conserve the two-sites basis. This condition is mandatory, otherwise the world

lines may break, yielding no statistical weights. Ruling out observables such as correlations of the type $\hat{S}_i^+ \hat{S}_j^-$.

With all the necessary conditions to perform measurements, we calculate expected values in the usual statistical manner using the trace operator and the density matrix of the system:

$$\langle \hat{O} \rangle = \mathrm{tr}\left(\hat{\rho}\, \hat{O} \right) \quad \text{with} \quad \hat{\rho} = \frac{e^{-\beta \hat{H}}}{Z}. \tag{16}$$

Using the same decomposition as in Eq. (8) and separating the observable as stated in Eq. (15), the expression for the expected value becomes

$$\langle \hat{O} \rangle = \lim_{M \to \infty} \frac{1}{Z} \, \mathrm{Tr}\left(e^{-\Delta\tau \hat{H}_A} e^{-\Delta\tau \hat{H}_B} \right)^M \\ \times \left(\hat{O}_A + \hat{O}_B \right), \tag{17}$$

where Z is defined by Eq. (13). Taking advantage of the cyclic properties of the trace, $\mathrm{Tr}(\hat{A}\hat{B}) = \mathrm{Tr}(\hat{B}\hat{A})$, we reorganize the above terms as

$$\langle \hat{O} \rangle = \lim_{M \to \infty} \frac{1}{Z} \mathrm{Tr}\left(e^{-\Delta\tau \hat{H}_A} e^{-\Delta\tau \hat{H}_B} \right)^{M-1} \\ \times \left(e^{-\Delta\tau \hat{H}_A} \hat{O}_A e^{-\Delta\tau \hat{H}_B} + e^{-\Delta\tau \hat{H}_A} e^{-\Delta\tau \hat{H}_B} \hat{O}_B \right). \tag{18}$$

Manipulating the last expression, we can transform it in terms of the classical configuration weights:

$$\langle \hat{O} \rangle = \lim_{M \to \infty} \frac{1}{Z} \sum_C \Omega\left(C \right) \left(\frac{\langle \sigma^0 | e^{-\Delta\tau \hat{H}_A} \hat{O}_A | \sigma^1 \rangle}{\langle \sigma^0 | e^{-\Delta\tau \hat{H}_A} | \sigma^1 \rangle} \right. \\ \left. + \frac{\langle \sigma^0 | e^{-\Delta\tau \hat{H}_B} \hat{O}_B | \sigma^1 \rangle}{\langle \sigma^0 | e^{-\Delta\tau \hat{H}_B} | \sigma^1 \rangle} \right), \tag{19}$$

in such a way that the observable is measured in one imaginary time slice, between $\langle \sigma^0 |$ and $| \sigma^1 \rangle$. Using again the cyclic properties of the trace, we can measure the observables at any arbitrary time slice $\langle \sigma^\alpha | - | \sigma^{\alpha+1} \rangle$ of the configuration. Hence, we average the observable through all the time slices:

$$\langle \hat{O} \rangle = \lim_{M \to \infty} \frac{1}{MZ} \sum_C \Omega\left(C \right) \\ \times \left(\sum_\alpha \frac{\langle \sigma^\alpha | e^{-\Delta\tau \hat{H}_{A(B)}} \hat{O}_{A(B)} | \sigma^{\alpha+1} \rangle}{\langle \sigma^\alpha | e^{-\Delta\tau \hat{H}_{A(B)}} | \sigma^{\alpha+1} \rangle} \right), \tag{20}$$

where imaginary-time and spatial periodic boundary conditions are implicit and the operators $\hat{H}_{A(B)}$ and $\hat{O}_{A(B)}$ depend on whether σ is even or odd. Next, doing algebraic manipulations on the last expression, we arrive to a general form for the expected value of a given observable

$$\langle \hat{O} \rangle = \lim_{M \to \infty} \frac{1}{MZ} \sum_C \Omega\left(C \right) \\ \times \left(\sum_{i,\alpha} \frac{\langle \sigma_{i,i+1}^{\alpha+1} | e^{-\Delta\tau \hat{H}_{i,i+1}} \hat{O}_{i,i+1} | \sigma_{i,i+1}^\alpha \rangle}{\langle \sigma_{i,i+1}^{\alpha+1} | e^{-\Delta\tau \hat{H}_{i,i+1}} | \sigma_{i,i+1}^\alpha \rangle} \right). \tag{21}$$

With this expression, it is clear that the measurement of expected values with this method is a weighted sum over the observables calculated in all the different possible effective classical configurations. Finally, expected values are simply evaluated as

$$\langle \hat{O} \rangle = \frac{1}{MZ} \sum_C \Omega(C) O(C), \tag{22}$$

where the expression in parenthesis in Eq. (21) is settled as $O(C)$. At last, as an example, we present expected values of three observables. The first one is the internal energy, which is given by

$$\langle \hat{H} \rangle = \frac{\sum_C \Omega\left(C \right) E\left(C \right)}{Z}, \tag{23}$$

where $E(C)$ is the classical mean energy defined by

$$E(C) = -\frac{1}{M} \frac{\partial \ln \Omega(C)}{\partial \Delta\tau}. \tag{24}$$

Another important observable is the magnetization, whose form becomes

$$\langle \hat{M} \rangle = \frac{1}{MZ} \sum_C \Omega\left(C \right) \left(\sum_{i,\alpha} M_i^\alpha \right), \tag{25}$$

where M_i^α are the classical matrix elements. Finally, other type of interesting measurements are the ones given by the occupation per site, determined as

$$\langle \hat{n}_{i,\sigma} \rangle = \frac{1}{MZ} \sum_C \Omega\left(C \right) \left(\sum_\alpha n_{i,\sigma}^\alpha \right), \tag{26}$$

where $\hat{n}_{i,\sigma}$ is the spin magnetic projection number operator in the i-th site.

4.1. Weighted sampling

Although we have a general expression and some particular ones to calculate different observables, we recall that it is impossible to sample all the classical configurations, hence we can not calculate the complete partition function. A solution is to use Monte Carlo sampling to obtain the most relevant configurations, *i.e.* the ones with the larger weight, to measure the observables statistically. For this weighted sampling, we use the Metropolis algorithm [40]. Here, we only give a brief description of it, for a more detailed review see [41].

The Monte Carlo procedure allows for stochastic evaluation of expectation values in the form of expression (22) with respect to the partition function in Eq. (14), by generating a Markov chain of configurations distributed like $\Omega(C)$. Therefore, we can compute the observables with an estimator

$$\langle O \rangle \approx \frac{1}{n} \sum_{j=1}^n O(C_j), \tag{27}$$

where n is the number of configurations generated through the Markov chain. In practice, the first γ configurations are discarded, where γ is the thermalization threshold that may vary depending on the physical model, we take the last 30% to perform measurements. There are two sufficient conditions to achieve the desired distribution [42]:

1. Ergodicity: Every possible configuration can be reached from any given configuration through a finite Markov chain. A priori, our system does not satisfy this due to the periodic boundary conditions imposed by the trace, but those vanish in the thermodynamic limit.

2. Detailed balance: The transition probabilities of the Markov chain must satisfy:

$$\frac{P_{\mu \to \nu}}{P_{\nu \to \mu}} = \frac{P_\nu}{P_\mu}, \tag{28}$$

where $P_{\mu \to \nu}$ is the probability of evolving from state μ to state ν and P_μ (P_ν) is the probability of being in state μ (ν).

One solution for the detailed balance condition is the Metropolis probability [40], which allows us to do local updates (respecting the boundary conditions) to generate a Markov chain of configurations and maximize their weight with the following transition rate

$$P_{\mu \to \nu} = \begin{cases} \frac{\Omega(W_\nu)}{\Omega(W_\mu)} & \Omega_\nu < \Omega_\mu, \\ 1 & \Omega_\nu \geq \Omega_\mu. \end{cases} \tag{29}$$

When the locally updated configuration has a more favorable weight (a larger weight) than the initial one, the update is accepted. However, if this is not the case, the update is not directly rejected, it still has a random acceptance probability.

5. Results and Discussion

We present the evolution of the weights of three different configurations, for a 1D chain with size $L = 10$ and the Trotter number $M = 100$, as a function of Monte Carlo steps (MCS); each MCS is given by a local update using the Metropolis scheeme to maximize the weight of an initial classical configuration. The interaction strength is set to $\theta = -0.85\pi$ for all the configurations, and the magnetic field D takes values 0.2, -0.2 and -0.9 and their weight evolutions are shown in Fig. 3 panels a), b) and c), respectively. As it can be seen, the evolutions present different behaviors and scales, this arises from the fact that the parameters have been chosen to yield in the Ising ferromagnetic phase for the panel a), the XY ferromagnetic phase for b) and finally the large-D phase in c). For a review of these quantum magnetic phases see [25].

The weight of any initial configuration given in all three of the previously described phases is maximized, thus allowing us to do a weighted sampling on the classical configurations to compute statistically the expected value of the set
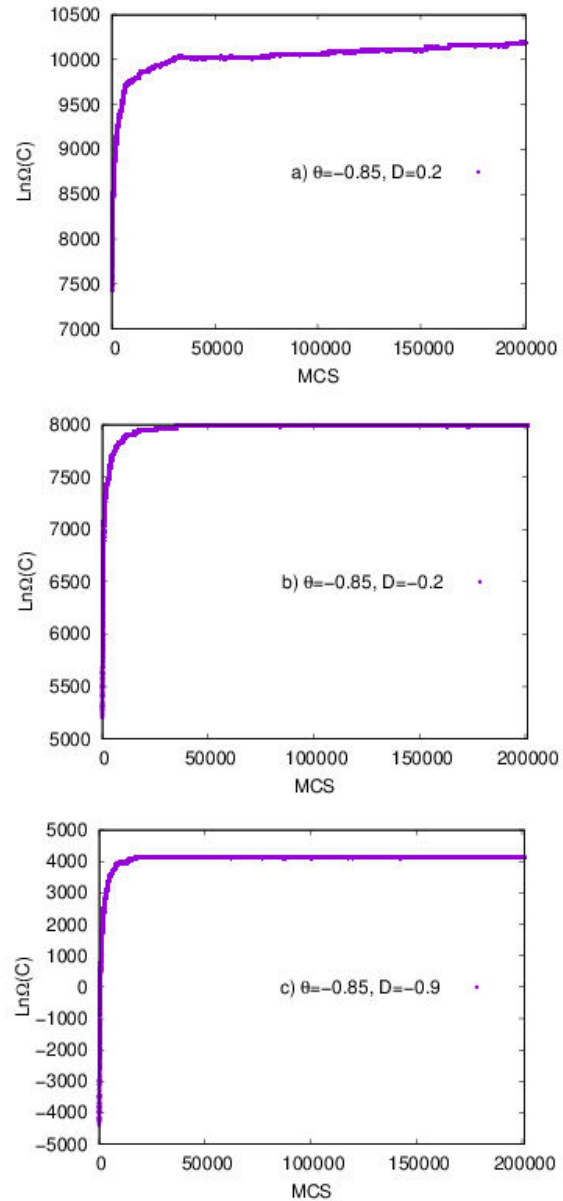

FIGURE 3. Weight as a function of Monte Carlo steps for three configurations in different phases: a) Ising ferromagnetic, b) XY ferromagnetic and c) Large-D.

of observables using an estimator. It is observed that $\gamma = 30\%$ is a good threshold, because all the presented weights have thermalized, meaning that the weight fluctuates around a mean value. For this thermalization to occur, the temperature of the system had to be taken at least as $T = 10^{-3}$ in units of $1/k_B$. Larger values would induce thermal fluctuations preventing the maximization of the weights.

6. Conclusions

We described the implementation of the world line Monte Carlo with local updates as a tool to solve lattice many-body quantum systems. We showed how with this method,

a d-dimensional quantum system is mapped into a d+1-dimensional effective classical system which can be sampled using the Metropolis algorithm to statistically measure a set of observables. The implementation was done particularly for the bilinear-biquadratic Heisenberg model with an external quadratic Zeeman field for spin-1 particles at ultralow temperatures. We present the maximization of the weights taken from the set of configurations for the three different ferromagnetic phases the model exhibits, *i.e.*, Ising ferromagnetic, XY ferromagnetic and large-D, for a 1D chain with periodic boundary conditions.

The maximization of the weights is a relevant and outstanding result towards statistical measurements of allowed physical observables. Hence, as a perspective, the measurement of observables such as the three described in this work, in order to characterize the magnetic phases of the system, is desirable.

Acknowledgments

1. M. Lewenstein, A. Sanpera, V. Ahufinger, B. Damski, A. Sen(De), U. Sen, *Adv. Phys.* **56** (2007) 243. https://doi.org/10.1080/00018730701223200

2. I. Bloch, J. Dalibar, W. Zwerger, *Rev. Mod. Phys.* **80** (2008) 885. https://link.aps.org/doi/10.1103/RevModPhys.80.885

3. D. Jaksch, C. Bruder, J. I. Cirac, C. W. Gardiner, P. Zoller, *Phys. Rev. Lett.* **81** (1998) 3108. https://doi.org/10.1103/PhysRevLett.81.3108

4. M. Greiner, O. Mandel, T. Esslinger, T. W. Hänsch, I. Bloch, *Nature* **415** (2002) 39. http://dx.doi.org/10.1038/415039a

5. C. N. Cohen-Tannoudji, *Rev. Mod. Phys.* **70** (1998) 707. https://doi.org/10.1103/RevModPhys.70.707

6. W. D. Phillips, *Rev. Mod. Phys.* **70** (1998) 721. https://doi.org/10.1103/RevModPhys.70.721

7. S. Chu, *Rev. Mod. Phys.* **70** (1998) 685. https://doi.org/10.1103/RevModPhys.70.685

8. E. A. Cornell, C. E. Wieman, *Rev. Mod. Phys.* **74** (2002) 875. https://doi.org/10.1103/RevModPhys.74.875

9. W. Ketterle, *Rev. Mod. Phys.* **74** (2002) 1131. https://doi.org/10.1103/RevModPhys.74.1131

10. D. J. Wineland, *Rev. Mod. Phys.* **85** (2013) 1103. https://doi.org/10.1103/RevModPhys.85.1103

11. S. Haroche, *Rev. Mod. Phys.* **85** (2013) 1083. https://doi.org/10.1103/RevModPhys.85.1083

12. M. Greiner, S. Fölling, *Nature* **453** (2008) 736. https://doi.org/10.1038/453736a

13. I. M. Georgescu, S. Ashhab, F. Nori, *Rev. Mod. Phys.* **86** (2014) 153. https://doi.org/10.1103/RevModPhys.86.153

14. T. L. Ho, *Phys. Rev. Lett.* **81** (1998) 742. https://link.aps.org/doi/10.1103/PhysRevLett.81.742

15. T. Ohmi, K. Machida, *J. Phys. Soc. Jpn.* **67** (1998) 1822. https://doi.org/10.1143/JPSJ.67.1822

16. M. Rizzi, D. Rossini, G. De Chiara, S. Montangero, R. Fazio, *Phys. Rev. Lett.* **95** (2005) 240404. https://doi.org/10.1103/PhysRevLett.95.240404

17. G. G. Batrouni, V. G. Rousseau, R. T. Scalettar, *Phys. Rev. Lett.* **102** (2009) 140402. https://doi.org/10.1103/PhysRevLett.102.140402

18. L. de Forges de Parny, F. Hébert, V. G. Rousseau, G. G. Batrouni, *Phys. Rev. B* **88** (2013) 104509. https://link.aps.org/doi/10.1103/PhysRevB.88.104509

19. L. E. Sadler, J. M. Higbie, S. R. Leslie, M. Vengalattore, D. M. Stamper-Kurn, *Nature* **443** (2006) 312. http://dx.doi.org/10.1038/nature05094

20. M. Vengalattore, S. R. Leslie, J. Guzman, D. M. Stamper-Kurn, *Phys. Rev. Lett.* **100** (2008) 170403. https://link.aps.org/doi/10.1103/PhysRevLett.100.170403

21. A. Imambekov, M. Lukin, E. Demler, *Phys. Rev. Lett.* **93** (2004) 120405. https://link.aps.org/doi/10.1103/PhysRevLett.93.120405

22. B. Capogrosso-Sansone, Ş. G. Söyler, N. V. Prokof'ev, B. V. Svistunov, *Phys. Rev. A* **81** (2010) 053622. https://link.aps.org/doi/10.1103/PhysRevA.81.053622

23. J. Jiang, L. Zhao, S. T. Wang, Z. Chen, T. Tang, L. M. Duan, Y. Liu, *Phys. Rev. A* **93** (2016) 063607. https://link.aps.org/doi/10.1103/PhysRevA.93.063607

24. P. A. Belov, A. A. Nazarov, A. O. Sorokin, *Phys. Rev. E* **95** (2017) 063308. https://doi.org/10.1103/PhysRevE.95.063308

25. K. Rodríguez, A. Argüelles, A. K. Kolezhuk, L. Santos, T. Vekua, *Phys. Rev. Lett.* **106** (2011) 105302. https://link.aps.org/doi/10.1103/PhysRevLett.106.105302

26. L. de Forges de Parny, F. Hebert, V. G. Rousseau, G. G. Batrouni, *Phys. Rev. B* **88** (2013) 104509. https://link.aps.org/doi/10.1103/PhysRevB.88.104509

27. L. de Forges de Parny, V. G. Rousseau, *Phys. Rev. A* **97** (2018) 023628. https://link.aps.org/doi/10.1103/PhysRevA.97.023628

28. J. J. García-Ripoll, M. A. Martin-Delgado, J. I. Cirac, *Phys. Rev. Lett*. **93** (2004) 250405. https://link.aps.org/doi/10.1103/PhysRevLett.93.250405

29. M. Troyer, F. Alet, S. Trebst, S. Wessel, *AIP Conf. Proc.* **690** (2003) 156. https://doi.org/10.1063/1.1632126

30. H. Fehske, R. Schneider, A. Weiße, *Computational Many-Particle Physics*, (Springer, Berlin Heidelberg 2008), pp. 277-353. https://doi.org/10.1007/978-3-540-74686-7

31. L. Pollet, *Rep. Prog. Phys*. **75** (2012) 094501. http://stacks.iop.org/0034-4885/75/i=9/a=094501

32. U. Schollwöck, *Rev. Mod. Phys*. **77** (2005) 259. https://doi.org/10.1103/RevModPhys.77.259

33. U. Schollwöck, *Ann. Phys*. **326** (2011) 96. https://doi.org/10.1016/j.aop.2010.09.012

34. H. Bethe, *Z. Phys* **71** (1931) 205. https://doi.org/10.1007/BF01341708

35. M. C. Gutzwiller, *Phys. Rev. Lett*. **10** (1963) 159. https://doi.org/10.1103/PhysRevLett.10.159

36. U. Schollwöck, J. Richter, D. J. J. Farnell, R. F. Bishop, *Quantum Magnetism*, (Springer, Berlin Heidelberg, 2004). https://doi.org/10.1007/b96825

37. M. Suzuki, *Progr. Theor. Exp. Phys*. **56** (1976) 1454. http://dx.doi.org/10.1143/PTP.56.1454

38. H. F. Trotter, *Proc. Amer. Math. Soc*. **10** (1959) 545. https://doi.org/10.1090/S0002-9939-1959-0108732-6

39. G. C. Wick, *Phys. Rev.* **96** (1954) 1124. https://doi.org/10.1103/PhysRev.96.1124

40. N. Metropolis, A. W. Rosenbluth, M. N. Rosenbluth, A. H. Teller, *J. Chem. Phys*. **21** (1953) 1087. https://doi.org/10.1063/1.1699114

41. M. E. J. Newman, G. T. Barkema, *Monte Carlo Methods in Statistical Physics*, (Oxford University Press, Oxford, 1999), pp. 19-85. https://doi.org/10.2307/2670314

42. H. G. Evertz, *Adv. Phys.* **52** (2003) 1. https://doi.org/10.1080/0001873021000049195